Linearity of Ca^{2+}-Doped $CeBr_3$ Scintillating Materials

Paul Guss*[a], Michael E. Foster,[b] Bryan M. Wong,[b] F. Patrick Doty,[b] Kanai Shah,[c] Michael Squillante,[c] Urmila Shirwadkar,[c] Rastgo Hawrami,[c] Josh Tower,[c] Thomas Stampahar,[a] and Ding Yuan[d]

[a]*National Security Technologies, LLC, Remote Sensing Laboratory–Nellis, P.O. Box 98521, M/S RSL-09, Las Vegas, NV 89193-8521, USA, gusspp@nv.doe.gov*

[b]*Sandia National Laboratories, California, Materials Chemistry Department, P.O. Box 969, Livermore, CA 94551-0969, USA;*

[c]*Radiation Monitoring Devices, Inc., 44 Hunt Street, Watertown, MA 02472, USA;*

[d]*National Security Technologies, LLC, P.O. Box 98521, Las Vegas, NV 89193-8521, USA*

ABSTRACT

The National Security Technologies, LLC, Remote Sensing Laboratory (RSL) developed an aliovalently calcium-doped cerium tribromide ($CeBr_3$:Ca^{2+}) crystal with a FWHM resolution of 3.2% at the ^{137}Cs 662 keV gamma energy. RSL completed a crystal assessment and Sandia National Laboratories calculated the predictive performance and physical characteristics using proven density functional theory (DFT) formalism. Results are reported for the work done to map the detector performance, characteristics, calcium doping concentration, and crystal strength. Preliminary scintillation measurements for this aliovalently calcium-doped $CeBr_3$ scintillator exhibit a slight blue shift in fluorescence emission at 371 nm excitation for $CeBr_3$. The structural, electronic, and optical properties of $CeBr_3$ crystals were investigated using the DFT within generalized gradient approximation. The calculated lattice parameters are in good agreement with the experimental data. The energy band structures and density of states were obtained. The optical properties of $CeBr_3$, including the dielectric function of photons per unit energy, were calculated. Specifically, we report excellent linearity with the aliovalent $CeBr_3$:Ca^{2+} crystal. Proportionality of light yield is one area of performance in which Ce-doped and Ce-based lanthanide

* phone 1 702 295-8095; fax 1 702 295-8648; nstec.com

halides excel. Maintaining proportionality is the key to producing a strong, high-performance scintillator. Relative light yield proportionality was measured for both doped and undoped samples of $CeBr_3$ to ensure no loss in performance was incurred by doping. The light output and proportionality, however, appear to be similar to $CeBr_3$. There was a reduced yield at low energy. Relative light yield proportionality measurements suggest that dopants do not significantly affect proportionality at higher energies. RSL completed additional testing and evaluation of the new crystal as well as the assessment of benchmarking spectroscopy. Results, which present energy resolution as a function of energy, are summarized. Typical spectroscopy results using a ^{137}Cs radiation source are shown for our crystallites with diameters <1 cm. We obtain 3.2% before packing the crystallite in a sealed detector container and 4.5% for the packaged crystallite. More spectra were obtained for ^{241}Am, ^{60}Co, ^{228}Th, and background to exemplify $CeBr_3$:Ca^{2+} over a broader energy range.

Index Terms: detector, resolution, scintillator materials, gamma-ray detector, cerium tribromide; $CeBr_3$; high-resolution detector; halides; rare-earth compounds; scintillator; gamma spectral comparison; resolution; aliovalent substitution

1. Background

The scintillation properties of $CeBr_3$ crystals grown with the divalent dopant Ca^{2+} are presented. Small diameter (up to ~1 cm) single crystals of $CeBr_3$ doped with Ca^{2+} have been grown at Dynasil Radiation Monitoring Devices, Inc. (RMD). The aliovalently calcium-doped cerium tribromide ($CeBr_3$:Ca^{2+}) crystals were prepared according to careful theoretical modeling and delivered to the Remote Sensing Laboratory (RSL) for assessment and evaluation (**Fig. 1**). $CeBr_3$:Ca^{2+} has a hexagonal crystal structure identical to uranium trichloride (UCl_3). Hexagonal crystals may fracture easily; therefore, their manufacturing yield is expected to be low, making the reliability of large crystals questionable [1,2]. Significant gains in the practical scale for $CeBr_3$ scintillators may be realized by increasing fracture toughness of the crystals [3]. Aliovalent substitution, in which a host ion is replaced with an ion of

different valence (e.g., Ca^{2+} for Ce^{3+} in $CeBr_3$) is a more potent method of strengthening than isovalent substitution (i.e., replacing a fraction of ions with like-valence ions). In this approach, the formation of intrinsic defects necessary to maintain charge neutrality results in complexes with long-range interactions in the crystal. The resulting increase in hardening rate can be explained in terms of elastic interaction with dislocations [4].

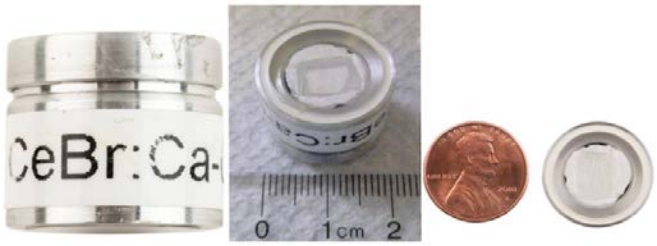

Fig. 1. Packaged scintillator of 0.2 atomic% Ca^{2+}-doped $CeBr_3$.

Because $CeBr_3$ already exhibits superior scintillation characteristics [5,6], the alloying element(s) used to strengthen the crystal must not degrade the scintillation properties. Aliovalent alloying provides more strengthening than isovalent alloying. The solid solution strengthening τ based on lattice distortions due to some small concentration of dopant can be approximated as

$$\tau = \gamma \bullet G c^{½}, \tag{1}$$

where G is the shear modulus, c is the concentration of solute in atomic fraction, and γ is a proportionality constant [7,8]. For spherically symmetric distortions, such as those found in isovalent alloying, γ typically takes on values that are significantly smaller than unity, on the order of 10^{-4} to 10^{-6}. For tetragonal lattice distortions, such as those created from solute atoms of a different valence, γ can be nearly unity. Therefore, aliovalent alloying is more effective for a given concentration of solute [8].

2. Experiment

A calcium-doped $CeBr_3$:Ca^{2+} crystallite was grown and packaged by RMD. Sandia National Laboratories (SNL) performed density functional theory (DFT) model calculations for a nominal doping (i.e., 2%) of calcium in $CeBr_3$. This helped assess what doping concentration would lead to changes in optical and mechanical properties. RMD assessed crystal growth strategies for performing growth with lower concentrations of calcium. SNL measured the calcium concentration by the inductively coupled plasma mass spectrometry.

RSL assessed the RMD crystal. RSL acquired spectra with different isotopes using the RMD crystal using the techniques described by Guss [3,9]. The emission spectrum for this crystallite is shown in **Fig. 2**. These results are consistent with recent findings [10]. The increase in doping level led to a slight blue shift in the emission spectrum. **Fig. 3** shows a light output measurement for the crystallite estimated at 62,000 photons per MeV based on comparison to the thallium-doped sodium iodide (NaI:Tl) light yield.

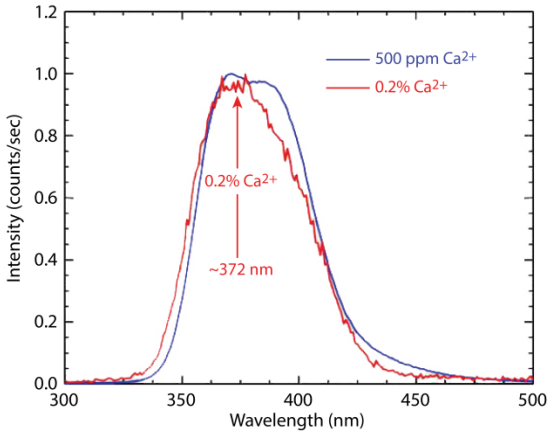

Fig. 2. Emission spectrum measured with 6 × 2 mm 0.2 atomic% Ca^{2+}-doped $CeBr_3$ crystal in the permanent canister compared to a similar measurement for a 500 ppm Ca^{2+}-doped $CeBr_3$ crystal.

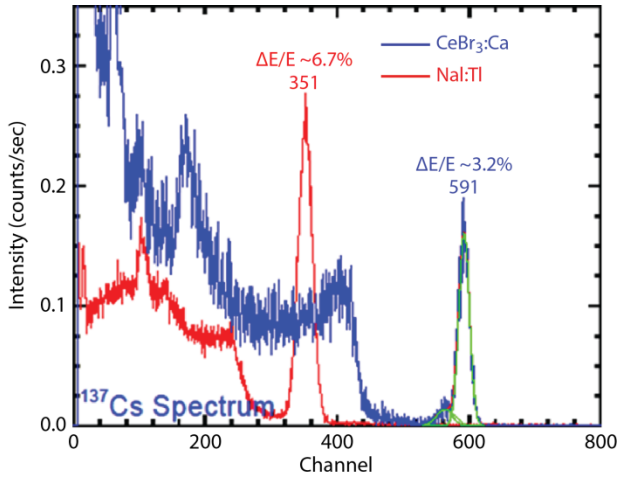

Fig. 3. Light output measurement relative to NaI:Tl indicates 62,000 photons per MeV for Ca^{2+}-doped $CeBr_3$ crystal.

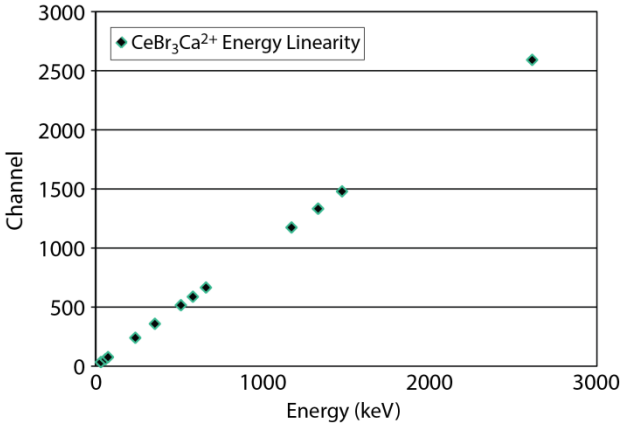

Fig. 4. Relative light yield proportionality of 0.2 atomic% Ca^{2+}-doped $CeBr_3$.

Proportionality of light yield is one area of performance where Ce-doped and Ce-based lanthanide halides excel. Maintaining proportionality is key to producing a strong, high-performance scintillator. Relative light yield proportionality was measured for both doped and undoped samples of $CeBr_3$ to ensure no loss in performance was incurred by aliovalently doping the crystal. The light output and proportionality, however, appear to be similar to $CeBr_3$. There was a reduced yield at low energy. Relative light yield proportionality measurements suggest that dopants do not significantly affect

proportionality at higher energies. A plot of light yield proportionality for a doped sample is shown in **Fig. 4**.

RSL completed additional testing and evaluation of the new crystal as well as the assessment of benchmarking spectroscopy data. Results are well summarized in **Fig. 4**, which present energy resolution as a function of energy. Typical spectroscopy results using a ^{137}Cs radiation source are shown in **Fig. 5** for our crystallites. We obtain 4.5% for the packaged crystallite. More spectra were obtained for ^{241}Am, ^{60}Co, ^{228}Th, and background to exemplify $CeBr_3$:Ca^{2+} over a broader energy range. The radiation source spectra were acquired for 3600 seconds with the radiation source in contact with the crystal face using typical source strengths of several μCi. The laboratory background acquisition time was 3×10^5 sec. Obviously, the packaging of the crystallite impacted the performance of $CeBr_3$:Ca^{2+}.

We have observed Ca^{2+} to be a most promising dopant, since it significantly reduces the nonproportionality and improves the energy resolution of pure $CeBr_3$. The nonproportionality was measured in the energy range from 32 keV up to 1274 keV. It has been observed that at 32 keV $CeBr_3$:Ca^{2+} deviates about 4% from the ideal case (10% for pure $CeBr_3$). We achieved an excellent energy resolution of 3.2% at 662 keV and light output of ~ 62,000 photons/MeV [11,12].

We sought to achieve ultralow activity and high strength cerium bromide scintillators through a program of refining and alloying with aliovalent strengthening agents (substituents with a different valence than the host lattice). $CeBr_3$ is a self-activated lanthanide scintillator, which has received considerable recent attention [13] due to proportionality and energy resolution for gamma spectroscopy far superior to NaI:Tl. Because the material possesses no intrinsic radioactivity, $CeBr_3$ has a high potential to outperform scintillators such as cerium-activated lanthanum tribromide or lanthanum-based elpasolites [14], making it an excellent candidate for gamma spectrometers for passive detection and identification of special nuclear material [15,16]. However, due to its hexagonal crystal structure (UCl_3), pure $CeBr_3$ can fracture during crystal growth, detector fabrication, and subsequent use under field conditions, thus impacting manufacturing yield and reliability for large crystals [2].

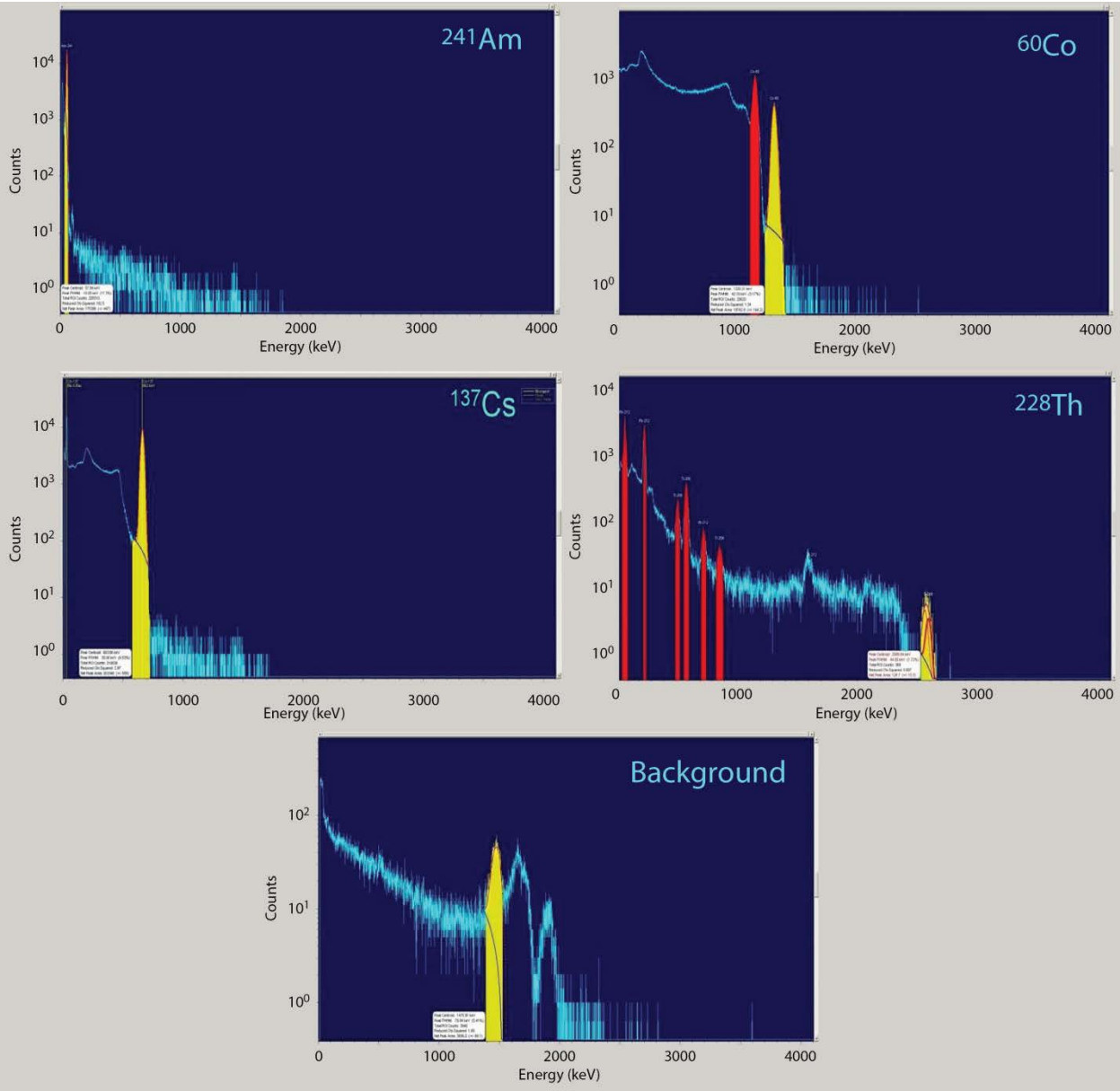

Fig. 5. ^{241}Am, ^{60}Co, ^{137}Cs, ^{228}Th, and background spectra with 1.9% Ca^{2+}-doped $CeBr_3$ in the permanent canister.

Aliovalent substitution, in which a host ion is replaced with an ion of different valence (e.g., Cd^{2+} for Ce^{3+} in $CeBr_3$) is a more potent method of strengthening than isovalent substitution (i.e., replacing a fraction of ions with like-valence ions). The formation of intrinsic defects necessary to maintain charge neutrality results in complexes with long-range interactions in the crystal. The resulting increase in

hardening rate can be explained in terms of elastic interaction (tetragonal distortion) with dislocations [4]. Concentration levels necessary to increase the yield strength by an order of magnitude may be in the 100–500 ppm range (0.01%–0.05%) for aliovalent substitution, whereas isovalent substitution may require 10%–50% to achieve the same effect.

For these reasons, aliovalent substitution was chosen to improve the strength of $CeBr_3$. SNL demonstrated success with this approach, achieving a dramatic reduction of fracture in aliovalent alloys compared with pure $CeBr_3$ crystals [8]. Prototype ingots were compounded with the addition of 2% of $CaBr_2$ added to a high-purity $CeBr_3$ charge in a closed ampoule before melting and solidification in a gradient-freeze process. Pure $CeBr_3$ ingots solidified under these conditions were severely fractured, yielding only centimeter-sized shards. The lesson learned was that 2% was too high of a charge for the calcium. Therefore, we needed to perform mass analysis of the material and recalculate the DFT with a lower charge of calcium. We also performed an assessment of the spectroscopic performance of the $CeBr_3$:Ca shards delivered by RMD to RSL.

The 2% calcium-doped $CeBr_3$:Ca crystallite was grown and packaged by RMD and delivered to RSL in late September 2012. Several minor tasks remained to complete characterization of the calcium-doped crystal. SNL performed DFT model calculations with less dilute doping (i.e., something less than 2%) of calcium in $CeBr_3$. This helped assess what doping concentration would lead to changes in optical and mechanical properties. RMD assessed crystal growth strategies for performing growth with lower concentrations of calcium. RSL assessed the spectroscopic performance of the crystal. RSL acquired spectra with different isotopes using the RMD crystal using the techniques described by Guss [3,17,18]. The emission spectrum for this crystallite is shown in **Fig. 2**. **Fig. 3** shows a light output measurement for the crystallite estimated at 62,000 photons per MeV based on comparison to the NaI:Tl light yield.

Figs. 3 and **6** present a comparison of the ^{137}Cs radiation source spectra and proportionality before and after packaging and sealing into the hermetically sealed canister sent to RSL. A slight degradation in performance is associated with the permanent package of the crystal. **Fig. 6** also illustrates the improvement in linearity achieved by doping the $CeBr_3$ with Ca^{2+}.

3. Calcium Concentration

We have measured the calcium concentration in the $CeBr_3$ by the inductively coupled plasma mass spectrometry (ICP-MS) technique from the crystals prepared by RMD. ICP-MS is a type of mass spectrometry capable of detecting metals and several non-metals at concentrations as low as one part in 10^{12} (part per trillion). SNL performed the ICP-MS. SNL also calculated a DFT model with less dilute doping (i.e., something less than 2%) of calcium in $CeBr_3$. SNL analyzed the concentration of calcium in the crystals. Referring to Table 1, we used the average calcium weight % concentration, x = 0.000214, in our complex of $Ce_{(1-x)}Ca_xBr_{(3-x)}$, to evaluate the formula for atomic percentage:

$$\text{Atomic \%} = 40.078x/[140.116\,(1 - x) + 40.078x + 79.904\,(3 - x)] = 0.00228 = 0.228\% \quad (2)$$

Based on our measurements, using three different samples (~0.2 grams), we have three consistent data sets indicating that the calcium concentration in these crystals is 0.0214 ±0.0102 wt.% (one σ) by weight, which corresponds to an atom percentage of 0.228 at.%. This value seems to be much less than the batch formulation. We do not know for certain if there is a solubility limit or a composition gradient in the ingot (sampling). Our data will be used to extract the solubility limit.

The objective of this portion of the task was to experimentally determine the solubility of $CaBr_2$ in the intrinsic scintillator $CeBr_3$. Our initial approach attempted equilibrium solid-state diffusion at several elevated temperatures for various amounts of time to allow Ca^{2+} to diffuse into the cerium bromide lattice, followed by chemical analysis to determine solubility limit and the activation energy for diffusion. However, this approach resulted in partial melting/fusion of the samples; therefore, a set of differential scanning calorimetric (DSC) measurements were performed and combined with our existing segregation data from crystal growth to build a working phase diagram in the $CeBr_3$-rich region.

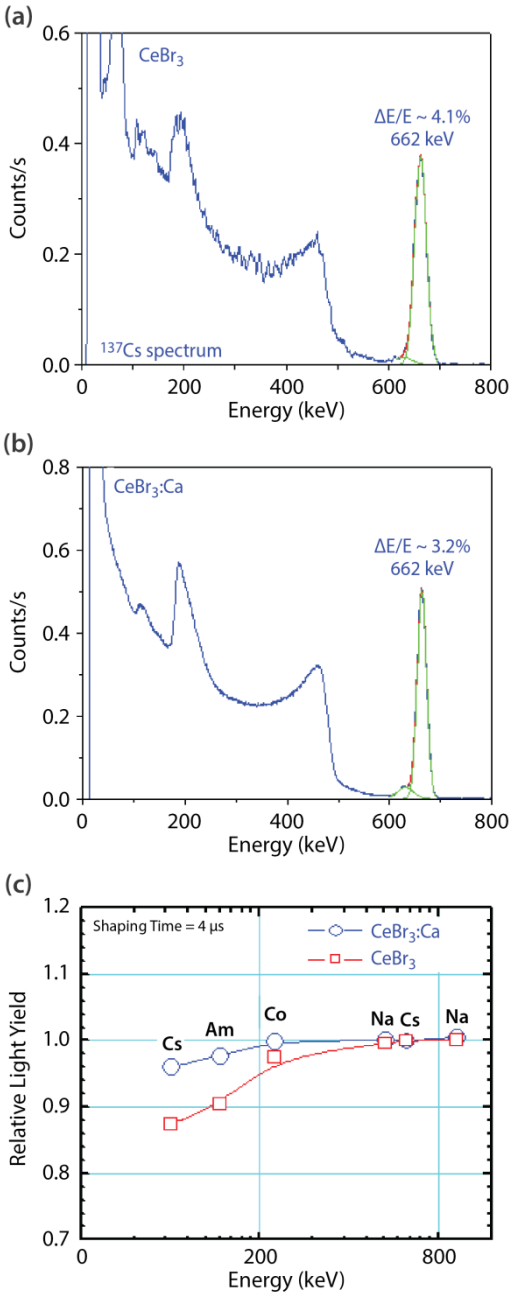

Fig. 6. (a) 662 keV spectrum with standard $CeBr_3$ with ~4% FWHM, (b) 662 keV spectrum with $CeBr_3$:Ca^{2+} with ~3.2% FWHM, (c) plots showing improved proportionality for $CeBr_3$:Ca^{2+} over standard $CeBr_3$.

The chemical analysis of three $CeBr_3$ samples from a nominal 2% ingot grown by RMD is summarized in **Table 1**. The ICP-MS was used to determine as-grown concentrations of calcium with

approximately 5% precision. Assuming the growth conditions were near equilibrium, an estimate for the segregation coefficient K_{eff} is $C_S/C_L = 0.11$. Therefore, the slope of the solidus line near 2% $CaBr_2$ in the liquid can be estimated by establishing a liquidus line from melting point data.

Table 1. ICP-MS assays for Ca(II)-doped $CeBr_3$; nominal composition 2 wt% $CaBr_2$ in $CeBr_3$

Sample	Calcium Concentration	95% Confidence Limit
#1	0.0238 wt%	0.0014 wt%
#2	0.0212 wt%	0.0015 wt%
#3	0.0192 wt%	0.0015 wt%

Table 2 is a tabulation of DSC data taken on samples in the composition range of 0%–10% $CaBr_2$ by mole. While the measured melting temperature T_m for the pure $CeBr_3$ sample appears anomalous and is in poor agreement with the literature, the mixtures show linear trends, including an apparent eutectic temperature T_e near 597ºC for calcium concentrations ≥2.35%.

Table 2. DSC results for $CeBr_3$-$CaBr_2$ mixtures in the range 0–10 mole %

Mole % $CaBr_2$	T_m	T_e
0	715.3ºC	–
0.2	732.1ºC	–
2.35	721.8ºC	598.3ºC
4.65	715.2ºC	595.4ºC
7.63	706.8ºC	596.2ºC
9.85	697.3ºC	597.0ºC

All results are plotted in **Fig. 7**, on which approximate solidus, liquidus, and eutectic lines have been constructed. Not plotted are some additional data taken at 20% and 30%, which indicate the liquidus

continues the near-linear trend. Note that our current experimental upper bound for the solid solubility is the data point at 2.35%, which must lie well within the α + β field, since the eutectic temperature T_e was detected. This concentration is considerably less than the intersection of the extrapolated solidus and the eutectic temperature; therefore, the solidus line is clearly nonlinear and probably exhibits retrograde solubility well below the melting point of pure $CeBr_3$, as is commonly observed for sparingly soluble impurities in other systems. This behavior can be characterized as a variation of the segregation coefficient with temperature, as analyzed by Hall [19]. For example, the maximum solid solubility for sparingly soluble impurities in silicon and germanium follow a simple empirical correlation with k_0, the limiting equilibrium segregation coefficient, as C_L approaches 0: $C_{S,max} = k_0/10$ [20]. Based on this relation, the solidus was arbitrarily extrapolated to $k_{eff}/10 = 1.1\%$ at the eutectic temperature to estimate the minimum extent of the eutectic line towards the $CeBr_3$ side of the phase diagram (**Fig. 7**).

It should be noted that the eutectic composition extrapolated from the points plotted is near 37% calcium; however, the nominal 20% and 30% data indicate it could be near 50%. More experiments are needed to accurately determine both the eutectic composition and the β phase, which could reasonably be expected to be a ternary such as $CaCeBr_5$ or Ca_2CeBr_7.

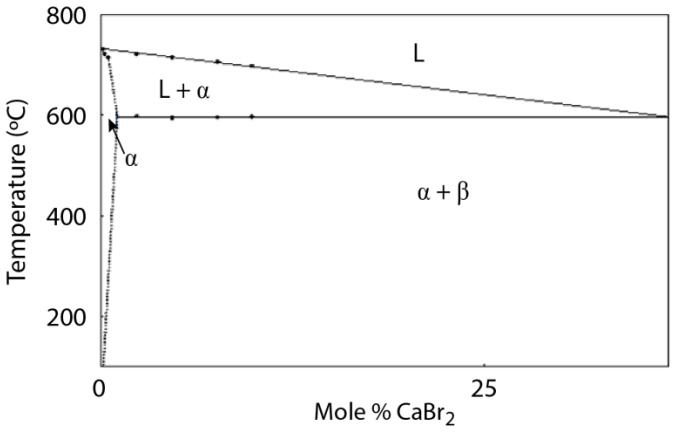

Fig. 7. Phase diagram for $CeBr_3$-$CaBr_2$

4. Discussion

SNL performed microhardness measurements to see if the aliovalent approach hardened the crystal as expected. Microhardness (Vickers hardness [21]) and indentation toughness of these samples were measured. Due to the size limitation, we could not obtain sufficient statistics and confidence on these measured values. Therefore, we do not report the results here. Future work should include studies in correlation between sheer strength and Ca^{2+} concentration.

Based on the recent literature on strengthening mechanisms [22], there are compelling requirements to research and several ideas, questions, and answers to share. Sinha's paper on aliovalent strengthening of CaF_2 attempts to determine mechanisms for low and high temperatures. Sinha and Nicholson [22] found that Y(III) gave an order of magnitude greater increase in critical resolve shear stress than Na(I). They conclude the long-range retarding force on dislocations at high temperature is likely due to the induced reorientation of Na(I)/F-vacancy or Y(III)/F-interstitial dipoles in the stress fields of moving dislocations (Snoek effect). This suggested role of the Snoek effect [22] is in accord with analysis of the athermal regime in recent papers on Y stabilized zirconia and other materials [5,13,24–30]. If the authors are correct that anion interstitials balance the charge for the higher valence cation, then the difference in strength may be related to the higher mobility of interstitials. The interstitial fluoride ion in CaF_2 may be more plausible than interstitial bromide; however, the $CeBr_3$ crystal structure does have large open channels. We examined whether the M(IV)/Br-interstitial seems like a feasible complex in $CeBr_3$. Because the athermal (high-temperature) regime is probably more important during crystal growth, future work should explore if it makes sense to place more emphasis on M(IV) cations silicon, tin, lead, titanium, zirconium, hafnium, rhenium, molybdenum, cerium, thorium, protactinium, uranium, neptunium, and plutonium.

5. Summary

To summarize, new DFT simulations demonstrate a capability for predicting properties of doped $CeBr_3$ materials that is unavailable elsewhere but is critically needed to study the property-limiting

valence phenomena in ionic compounds. During this project, we assessed concentrations and the solubility limit. RSL benchmarked the Ca^{2+}-doped $CeBr_3$ crystal. The Ca^{2+}-doped $CeBr_3$ crystal has improved energy resolution (i.e., 3.2%) and linearity over the pure $CeBr_3$ crystal.

Acknowledgment

Marlene Bencomo (University of New Mexico, Albuquerque) assisted with IC-PMS analysis. This manuscript has been authored by National Security Technologies, LLC, under Contract No. DE-AC52-06NA25946 with the U.S. Department of Energy and supported by the Site-Directed Research and Development Program. The United States Government retains and the publisher, by accepting the article for publication, acknowledges that the United States Government retains a non-exclusive, paid-up, irrevocable, world-wide license to publish or reproduce the published form of this manuscript, or allow others to do so, for United States Government purposes.

References

[1] F. P. Doty, et al., *Proc. SPIE* **6707** (2007) 670705:1–11.

[2] F. P. Doty, et al., *Proc. Mat. Res. Soc.* **1038** (2008) 1–8.

[3] P. Guss, et al., *Site-Directed Research and Development*, FY 2012, National Security Technologies, LLC, Las Vegas, Nevada, 2013, 11–19.

[4] B. J. Pletka, et al., *Physica Status Solidi* **39**, 1 (1977) 301–311.

[5] K. S. Shah, et al., *IEEE Trans. Nucl. Sci*. **52**, 6 (2005) 3157–3159.

[6] S. Ra, et al., *IEEE Trans. Nucl. Sci.* **55**, 3 (June 2008) 1221–1224.

[7] T. H. Courtney, *Mechanical Behavior of Materials*, 2nd edition, Waveland, Long Grove, Illinois, 2000, 232.

[8] M. J. Harrison, et al., *Proc. SPIE* **7806** (2010) 78060M–78060M-14.

[9] P. P. Guss, et al., *Nevada National Security Site–Directed Research and Development*, FY 2010, National Security Technologies, LLC, Las Vegas, Nevada, 2011, 55–64.

[10] F. G. A. Quarati, et al., *Nucl. Instrum. Methods Phys. Res. A* (2013) http://dx.doi.org/10.1016/j.nima.2013.08.005.

[11] P. Guss, et al., *Site-Directed Research and Development*, FY 2013, National Security Technologies, LLC, Las Vegas, Nevada (2014) 221–234.

[12] U. Shirwadkar, et al., *Proceedings of the 20th Conference on Room-Temperature Semiconductor X- and Gamma-Ray Detectors*, IEEE, Seoul, South Korea (2013) N-4.

[13] K. S. Shah, et al., *IEEE Trans. Nucl. Sci.* **52**, 6 (2005) 3157–3159.

[14] P. P. Guss, et al., *Nucl. Instrum. Methods Phys. Res. A* **608**, 2 (2009) 297–304.[15] K. S. Shah, et al., *IEEE Trans. Nucl. Sci.* **51**, 5 (2004) 2395–2399.

[16] P. P. Guss, et al., *Proc. SPIE* **7805** (2010) L-1.

[17] P. P. Guss, et al., *Nevada National Security Site–Directed Research and Development*, FY 2010, National Security Technologies, LLC, Las Vegas, Nevada (2011) 55–64.

[18] P. P. Guss, et al., *J. Appl. Phys.* **115**, 3 (2014) 034908-1.

[19] R. N. Hall, *J. Phys. Chem. Solids* **3**, 1–2 (1957) 63–73.

[20] S. Fischler, *J. Appl. Phys.* **33**, 4 (1962) 1615.

[21] R. L. Smith and G. E. Sandland, *Proceedings of the Institution of Mechanical Engineers*, **I** (1922) 623–641.

[22] M. N. Sinha and P. S. Nicholson, *J. Mat. Sci.* **12**, 7 (1977) 1451–1462.

[23] J. Snoek, *Physica* **8**, 7 (1941) 711–733.

[24] D. Baither, et al., *Mat. Sci. Eng.* **A233** (1997) 75–87.

[25] D. H. Lassila, et al., *Metallurgical and Materials Transactions* **33A** 11 (November 2002) 3457–3464.

[26] C. Mercer, et al., *Proc. R. Soc. A* **463** (8 May 2007) 1393–1408, http://www.materials.ucsb.edu/MURI/papers/Merceretal_PRS07.pdf, accessed December 12, 2013.

[27] S. Armengol, Latin American Congress on Biomedical Engineering 2007, Bioengineering Solutions for Latin America Health, *IFMBE Proceedings* **18** (2008) 671–675.

[28] H. Martin and R. Pippan, *Materials Science Forum*, Trans Tech Publications, Switzerland **584-586** (2008) 938–943.

[29] L. Taherabadi, et al., *J. European Ceramic Soc.* **28** (2008) 271–376.

[30] Y. Gan, et al., *ASME 2010 8th International Conference on Fuel Cell Science, Engineering and Technology*, Brooklyn, New York, USA, June 14–16, 2010, doi: 10.1115/FuelCell2010-33194, Paper No. FuelCell2010-33194 **2** (2010) 153–158.